International Symposium
On Turbulence and Shear Flow
Phenomena (TSFP-8)
August 28 - 30, 2013 Poitiers, France

INVESTIGATION OF THE MIXING LAYER IN A SLIGHTLY UNDEREXPANDED SUPERSONIC JET BY PARTICLE IMAGE VELOCIMETRY

Benoît André, Thomas Castelain, Christophe Bailly
Laboratoire de Mécanique des Fluides et d'Acoustique
Ecole Centrale de Lyon
36 avenue Guy de Collongue, 69134 Ecully Cedex, France
thomas.castelain@ec-lyon.fr

ABSTRACT

A slightly underexpanded supersonic jet at a Mach number M_j of 1.10 is studied experimentally. Schlieren visualizations and particle image velocimetry are applied in order to characterise the shock-cell structure and turbulence in the mixing layer, which are the two elements at the origin of the shock-associated noise emitted by such a jet. It is found in particular that the velocity gradients typical of the shock-cell structure still exist in the subsonic part of the mixing layer. From the evaluation of some turbulence properties (turbulence level, momentum thickness and spatial correlation), it is shown that the jet behaves very similarly to jets at high subsonic Mach numbers. It is believed that such data could shed light on the shock-associated noise source.

INTRODUCTION

The commercial aircraft powered by turbofan engines exhaust slightly underexpanded supersonic jets at cruise conditions, characterised by the presence of a shock-cell pattern in the jet plume. The interaction in the mixing layer between the turbulence and the shock-cell system is responsible for the so-called shock-associated noise component of jet noise, which is in addition to the ever present turbulent mixing noise. Shock-associated noise is made up of two distinct parts : a tonal one, referred to as screech, and a broadband one (the broadband shock-associated noise).

While extensive static pressure measurements have been performed to characterise the shock-cell structure (*e.g.*, Norum & Seiner (1982)), detailed accounts of the turbulence in imperfectly expanded jets are scarce. Seiner & Norum (1980) measured turbulence levels and spectra using a hot film probe. Panda & Seasholtz (1999) obtained the coherent part of the density fluctuation in choked jets using the Rayleigh scattering technique and related this to the screeching process. Several studies applied particle image velocimetry (PIV) to these flows. Alkislar *et al.* (2003) separated the random from the coherent turbulent motion in the mixing layer of a screeching rectangular jet using stereoscopic PIV, and pinpointed the relation between coherent vortices and screech generation. Bridges & Wernet (2008) applied high-speed PIV to screeching and non-screeching supersonic jets, mainly focusing on turbulence spectra.

The objective of the present experimental study is to focus on some properties of the turbulence and the shock-cell structure in the mixing layer of a slightly underexpanded jet, with the ultimate goal of clarifying the broadband shock-associated noise generation process. Particle image velocimetry is thus applied to a jet at an ideally expanded Mach number $M_j = 1.10$. To begin with, the strength of the shock-cell structure in the mixing layer is estimated. Then, a study of the turbulence in this jet is reported. It addresses the turbulence levels, the mixing layer thickness, the location of the sonic line and the spatial correlations.

EXPERIMENTAL METHODS

The facility employed in the present work has already been used to study single-stream supersonic jets (André *et al.* (2013*b*)) as well as co-axial jets (André *et al.* (2011)). The configuration considered here is the latter one, with the outer stream set at a Mach number of 0.05 to seed the surroundings of the inner, supersonic jet, during the PIV measurements.

The supersonic jet flow originates from a continuously operating compressor mounted upstream of an air drier. It exhausts through a round, contoured and convergent nozzle of diameter $D = 38.7$ mm. Since the underexpanded jets exiting typical turbofan engines of civil aircraft do not seem to emit screech, it appears relevant to eliminate it in the small-scale study. For that purpose, a screech-suppressing nozzle is employed: shallow notches are cut into its lip. As indicated in a previous study (André *et al.* (2013*a*)), this nozzle non-intrusively suppresses screech. The reservoir temperature T_t is measured upstream of the exit. Here, the jets are unheated and $T_t \approx 30^\circ$C. The nozzle pressure ratio (NPR), defined as the ratio between jet stagnation pressure and ambient pressure, is set by measuring the wall static pressure fifteen nozzle diameters upstream of the exit.

A conventional Z-type schlieren system is used to visualise the flow. It consists of a light-emitting diode, two 203.2 mm-diameter f/8 parabolic mirrors, a straight knife-edge set perpendicular to the flow direction and a high-speed Phantom V12 CMOS camera.

Particle image velocimetry has also been applied to measure the velocity in a plane containing the jet axis and a notch. Illumination is provided by a pulsed double-cavity Nd:YLF Quantronix Darwin Duo laser. The sheet thickness is 1.7 mm $\pm$ 0.3 mm. The supersonic jet is seeded with olive oil by means of custom-designed Laskin nozzle generators. The mean particle size is known to be around 1 μm. The secondary flow is seeded by smoke. Both seeding devices are mounted far enough upstream of the exit so that the particle concentration in each flow is approximately uniform.

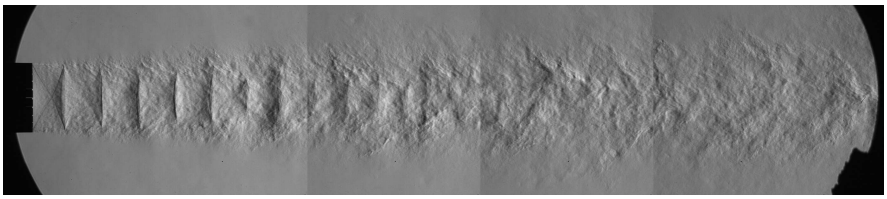

Figure 1. Schlieren image of a jet at $M_j = 1.10$. The picture is made up of five uncorrelated spark images (exposure time of 4 μs) recorded at different axial locations.

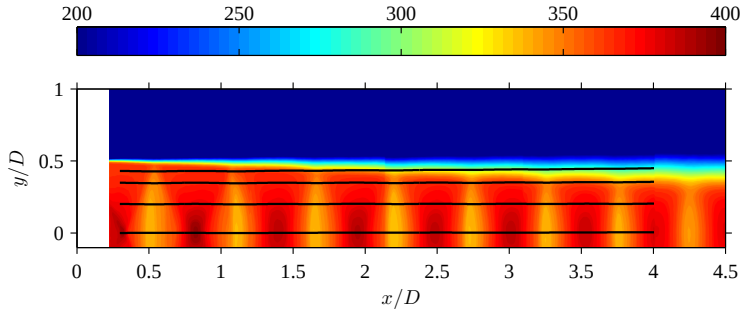

Figure 2. Cartography of the mean velocity $v = \sqrt{\overline{v_x}^2 + \overline{v_y}^2}$ (m.s^{-1}) for $M_j = 1.10$ (v_x and v_y are the longitudinal and transverse velocity components, respectively, and the overbar denotes the ensemble averaged value). The horizontal lines represent mean flow streamlines.

Two CMOS cameras of sensor size 1280×800 pixels^2 are set side by side to double the field of view available. The acquisition frequency of the image pairs is 500 Hz and the magnifying factor for each camera is about 0.05 mm/pixel. The delay between the images of each pair is set to 3 μs. The PIV set-up is mounted on a frame which can be translated in the jet direction. For each position, a length of about two jet diameters is viewed by the camera system. An axial extent of 12 D is studied here, meaning that the entire field has been acquired in six parts. For each new location of the frame, calibration of the camera images is performed using a three-dimensional LaVision plate, the jet operating conditions are reset and 2000 image pairs are recorded. Vector field calculation is performed by a multigrid FFT-based technique using the LaVison DaVis 7.2 software. In all but the last iteration, the calculation is a two-step process; a 25%-overlap of the interrogation windows is set and no window ponderation is used. For the last iteration, three computational steps are set, as well as a 50%-overlap and a Gaussian window ponderation. The final correlation windows are of size 8×8 pixels^2, leading to a vector density of one every 0.2 mm, or approximately 190 vectors across the supersonic jet diameter.

RESULTS

In order to introduce the shock-cell structure typical of underexpanded supersonic jets, a spark schlieren image of the jet at $M_j = 1.10$ is presented in figure 1. Owing to the orientation of the knife-edge in the schlieren set-up, longitudinal gradients of density are visualised here. The well-known quasi-periodic shock-cell pattern is visible. The light (dark) regions correspond to expansion (compression) regions (see Panda & Seasholtz (1999) or André *et al.* (2013*b*)). Turbulent fluctuations are also visible in this picture. The fact that they even appear in the jet core region is a result of the integration of the density gradients across the entire jet.

Shock-cell structure in the mixing layer

The shock-cell structure being directly responsible for the shock-associated noise emission, it is important to quantify the strength of the mean flow gradients near the mixing layer. Usually, pressure measurements are used for that purpose (Norum & Seiner (1982)) but they are generally confined to the jet core. Here, we deduce from the velocity map the gradients in the mixing layer and compare them to those existing in the jet core.

A map of the mean velocity is presented in figure 2, along with calculated mean flow streamlines, which reach from the first to the seventh shock cell. It is believed that the latter is representative of the downstream shock cells responsible for the emission of broadband shock-associated noise (Seiner & Yu (1984)). The mean velocity on these streamlines, which are almost straight at this low underexpansion, is shown in figure 3 (a), while the computed gradients of the mean velocity along the streamlines are displayed in (b) (in the latter figure, the negative peak near $x/D = 2$ comes from the connection between two separate fields of view). It is visible that the gradients wear off when moving downstream or toward the mixing layer. Hence, they remain small in the entire flow, and therefore, that is also the case in the region of production of broadband shock-associated noise.

Turbulence in the mixing layer

Turbulence levels To begin with, the turbulence levels measured in the mixing layer of the jet studied are analysed. Turbulence being mainly produced by velocity gradients, the ratios of the root-mean-square velocity components (written σ_x and σ_y for v_x and v_y) over the velocity difference ΔU between the supersonic jet and the low-speed co-flow are formed to provide indicators of turbulence levels. Since underexpanded supersonic jets are not uniform, it is not obvious which velocity is to be considered to compute ΔU. A mean velocity is chosen here, about which the axial velocity oscillates in the shock-cell structure.

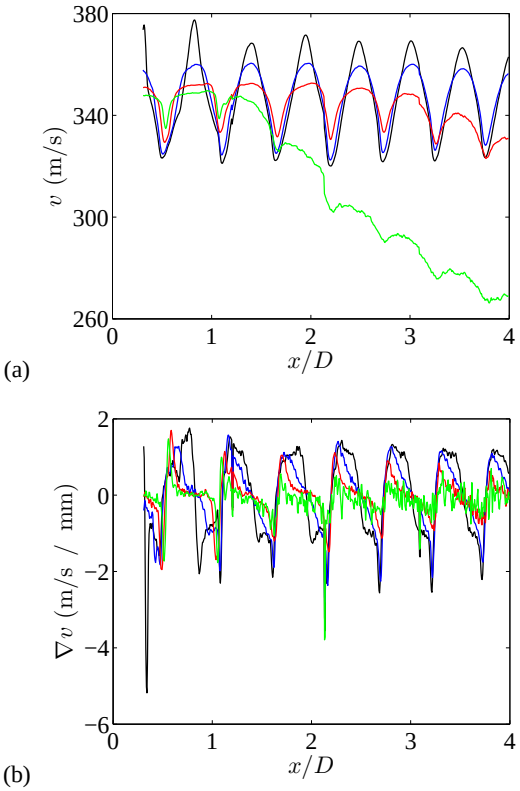

Figure 3. (a) Mean velocity profiles measured on the mean streamlines depicted in figure 2, (b) velocity gradients on the same streamlines; $M_j = 1.10$. The radial station of the streamlines at their upstream location are $y/D = 0$ (—), 0.2 (—), 0.35 (—), and 0.43 (—).

Turbulence levels are plotted in figure 4 on the lines of peak fluctuations for v_x. The turbulence intensities are seen to be quite flat, except very near the nozzle exit. They reach 16% for the longitudinal velocity, while the levels associated with the transverse component are between 10% and 11%. These values are in good agreement with what is observed in subsonic jets. Davies *et al.* (1963) measured with a hot wire probe peak turbulence levels of 16% in the mixing layer of round jets of Mach numbers lower than 0.6. Fleury (2006) obtained longitudinal profiles of turbulence intensity which are also flat and show about the same values as the present ones, for jet Mach numbers of 0.6 and 0.9. The results of Jordan *et al.* (2002) and Kerhervé *et al.* (2004), obtained by laser Doppler velocimetry for a jet Mach number of 0.9 as well as in an imperfectly expanded jet at $M_j = 1.2$, respectively, also suggest that the fluctuations do not depend on the axial location. It seems therefore that the shock-cell structure has little influence on the turbulence levels at this small degree of underexpansion. This conclusion has already been reached by Seiner & Norum (1980) from the comparison of fluctuation spectra between one underexpanded jet and a fully expanded jet of same M_j.

Momentum thickness The mixing layer momentum thickness is now assessed, as it is the relevant parameter for studying the stability of shear layers (Michalke (1965)). It will also provide a useful length scale for the following analysis.

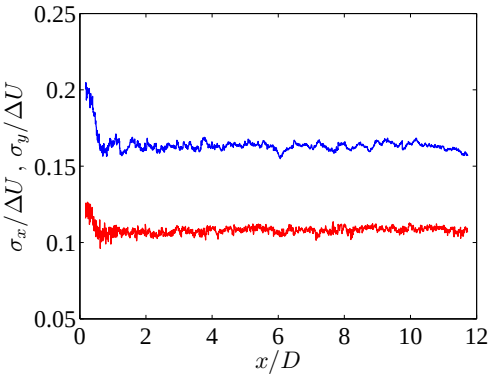

Figure 4. Longitudinal and transverse turbulence levels in the mixing layer, $M_j = 1.10$. — $\sigma_x/\Delta U$, — $\sigma_y/\Delta U$.

The momentum thickness δ_θ is written

$$\delta_\theta = \frac{1}{[\overline{v_x}(y_i) - \overline{v_x}(y_o)]^2} \int_{y_i}^{y_o} [\overline{v_x}(y) - \overline{v_x}(y_o)]\,[\overline{v_x}(y_i) - \overline{v_x}(y)]\,dy \qquad (1)$$

where y_i and y_o are the mixing layer limits inside and outside the supersonic jet. So as to properly define these boundaries, the fluctuation data obtained by the PIV are used. For each axial station, the radial location of the maximum root-mean-square value of the axial velocity fluctuations is determined. In the high- and low-velocity side of the flow, the fluctuation minima are searched. For each side, the mixing layer boundary is defined as the location where the root-mean-square velocity has decreased to 0.1 times the difference between the maximum and the minimum of the fluctuations. Finally, the integration of equation (1) is performed between these two limits, y_i and y_o. It has been verified that the precise value of the arbitrary threshold, taken at 0.1, had little effect on the estimation of δ_θ.

Another estimation of mixing layer thickness can be expressed $\delta = y_o - y_i$, and it was found that $\delta \approx 7.5\,\delta_\theta$.

The mixing layer growth (not shown here) is linear beyond the first diameter, which is characteristic of fully turbulent mixing layers (Troutt & McLaughlin (1982)). The numerical values of the slope is 0.0199. As a comparison, the growth rates measured by Fleury *et al.* (2008) in subsonic jets at Mach numbers of 0.6 and 0.9 are 0.0289 and 0.0265, respectively. The present result is thus consistent with subsonic values.

Position of the sonic line in the mixing layer Local Mach numbers can be inferred from the PIV data if it is assumed that the total temperature is uniform in the jet and equal to the reservoir temperature, by the formula

$$M = \left\{ \frac{v^2}{\gamma r T_t - v^2\,(\gamma - 1)/2} \right\}^{1/2} \qquad (2)$$

where M is the local Mach number, v the mean velocity, T_t the reservoir temperature, $\gamma = 1.4$ and $r = 287.06$ J/kg/K. The sonic line is then easily deduced and its location relatively to the mixing layer boundaries is studied here. The total temperature uniformity can be assumed because the

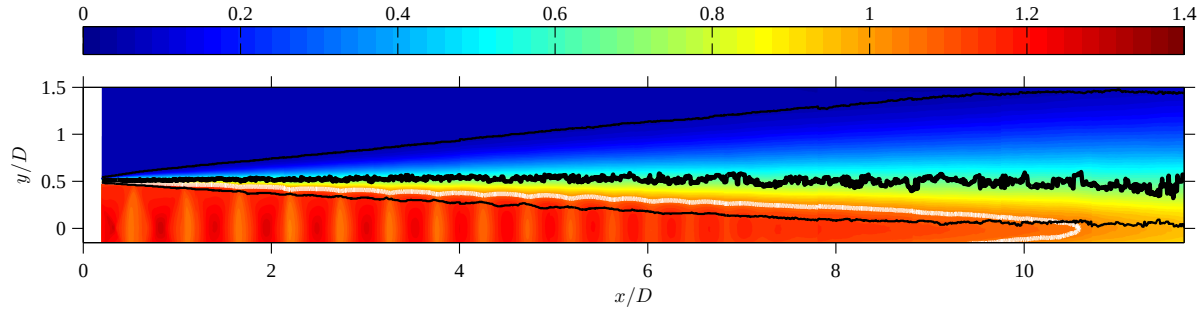

Figure 5. Map of the local Mach number obtained from the PIV data for $M_j = 1.10$. The thin black lines represent the boundaries of the mixing layer; the thick black line shows the location of maximum fluctuations of axial velocity; the white line is the sonic line.

jets are unheated, meaning that the total temperature inside the supersonic jet is very close to that of the low-speed co-flow. Furthermore, it was checked that the total temperature only had a limited effect on the results presented in the following.

A map of the local Mach number for the jet at $M_j = 1.10$ is presented in figure 5. Also included on the cartography are the locations of the mixing layer boundaries y_i and y_o, of the mixing layer centre, determined as the location where the axial velocity fluctuations are the strongest, and of the sonic line. It is obvious from figure 5 that most of the mixing layer is at subsonic conditions, and that the supersonic part is very thin. Moreover, the mixing layer centre lies well inside the subsonic mixing layer. The locations of mixing layer centre and boundaries relatively to the sonic line are shown in figure 6. y_s denotes the location of the sonic line, while y_c that of the centre of the mixing layer. The curves are truncated at $x/D = 8$ since the shock-cell structure ends approximately there. The observations made from figure 5 are well identified on this plot. Additionally, the shock-cell pattern extends into the subsonic part of the mixing layer: for example, the streamline at $y/D = 0.43$ in figure 3 lies in the subsonic part of the mixing layer for $x/D > 2$ and the mean velocity is still oscillating downstream. Hence, it appears that some part of the shock-associated noise may be emitted by the subsonic side of the mixing layer, and even a non negligible one in such a case. This belief contrasts with the modelisations of the BBSAN mechanism proposed by Harper-Bourne & Fisher (1973) and Seiner *et al.* (Seiner & Norum (1980); Seiner & Yu (1984)), who explain the shock-associated noise emission by the interaction between oblique shocks and the turbulence in the supersonic part of the mixing layer. In order to locate more precisely the source of BBSAN, a volumetric model of the sound sources, like that of Morris & Miller (2010), could be applied after estimation of some of the inputs not provided by our PIV measurements.

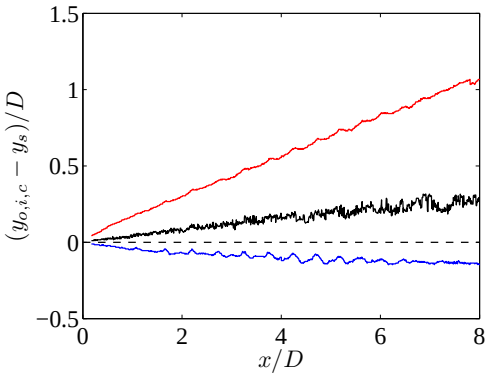

Figure 6. Location of the mixing layer boundaries and mixing layer centre relatively to the sonic line ($M_j = 1.10$). — $(y_c - y_s)/D$, — $(y_i - y_s)/D$, — $(y_o - y_s)/D$. The dashed horizontal line marks the sonic line location ($y = y_s$).

Spatial correlations Spatial correlations are computed from the velocity fields in order to obtain information on the size, shape and orientation of the turbulent structures in the mixing layer. The coefficient of space-time correlation is written

$$R_{ij}(\vec{x}, \vec{\xi}, \tau) = \frac{\overline{v_i'(\vec{x}, t)\, v_j'(\vec{x} + \vec{\xi}, t + \tau)}}{\sigma_i(\vec{x})\, \sigma_j(\vec{x} + \vec{\xi})} \qquad (3)$$

where the indexes i and j represent the velocity component, v_i' denotes the fluctuations of v_i, $\vec{x}$ is the reference point, $\vec{\xi}$ is the separation vector and τ is the time delay. Ensemble averages are calculated over the 2000 fields acquired. The indexes 1 and 2 will denote the axial and transverse directions, respectively. In the following, only spatial correlations are calculated, so that $\tau = 0$.

Cross-correlations R_{11} and R_{22} have been estimated while moving the reference point on the horizontal line $y/D_j = 0.5$, with D_j the fully expanded jet diameter, slightly larger than D. This is done to account for the expansion of underexpanded jets. It has been checked however that the precise location of the reference points did not have a strong influence on the results. Examples of correlation plots are shown in figure 7 for $M_j = 1.15$; they have much the same shape at $M_j = 1.10$.

From R_{ii}, $i \in (1,2)$, it is possible to calculate the correlation length scale of v_i' in the direction k, $k \in (1,2)$, by

$$L_{ii}^{(k)}(\vec{x}) = \frac{1}{2} \int_{-\infty}^{+\infty} R_{ii}(\vec{x}, \xi_k)\, \mathrm{d}\xi_k \qquad (4)$$

where ξ_k is the separation distance in the direction k. In practice, the integration is performed over a finite interval. Here, it is made until the correlation contour of level 0.1 to avoid the low correlation domain which can be noisy; in any case, the integration limit has no large influence on the

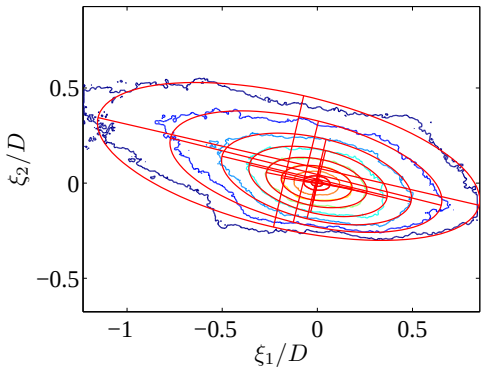

Figure 7. Example of a correlation contour R_{11} ($M_j = 1.15$, $y/D_j = 0.5$ and $x/D = 9$). The contours represent the correlation levels 0.1 to 0.9 in 0.1 step. The elliptical fits will be used below.

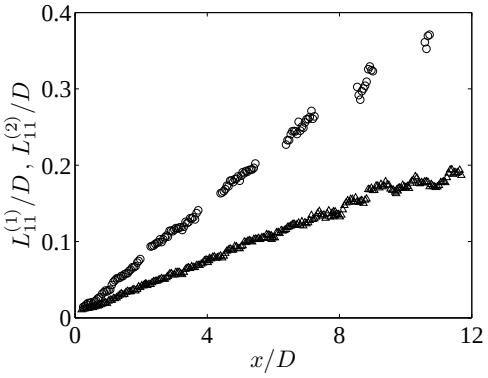

Figure 8. Integral length scales $L_{11}^{(k)}/D$ ($M_j = 1.10$). ○ $L_{11}^{(1)}$, △ $L_{11}^{(2)}$.

numerical values, and it has to be noted that integral length scales are merely order-of-magnitude estimates.

The length scales $L_{11}^{(k)}$ are shown in figure 8. They are seen to grow linearly with the downstream distance, as it is the case for subsonic jets (Laurence (1956); Davies *et al.* (1963); Fleury *et al.* (2008)). The estimates of $L_{22}^{(k)}$ are not shown here but they also grow linearly. Some data in the curve of $L_{11}^{(1)}$ are missing because of the limited axial extension of each field of view. Thus, the centered integration of $L_{11}^{(1)}$ becomes impossible near the field junctions as the structures grow.

Since the growth of both the length scales and the mixing layer thickness is linear, the ratios of the slopes of these two quantities are formed. The ratios $L_{11}^{(1)}/\delta_\theta$ and $L_{11}^{(2)}/\delta_\theta$ amount to 1.76 and 0.83, respectively. These values are not far from the approximate ratios of 2 and 1 observed by Fleury *et al.* (2008).

The shape of the correlation contours is now examined. The contour shown in figure 7 suggests that the turbulent structures have an elliptical shape, which has already been pinpointed by Mahadevan & Loth (1994) or Fleury *et al.* (2008). In order to quantitatively analyse the contours, ellipses have been fitted to them. The result of this can be viewed in figure 7. In the following, only contours of levels 0.3 to 0.8 are considered. Indeed, the contours of lower correlation level are generally more irregular and those of higher correlation are too small for a proper analysis. For each fitted contour, the inclination, the axis sizes and the excentricity of the ellipse have been obtained. The inclination is defined as the angle between the jet axis and the ellipse major axis. Noting a and b the length of the major and minor axes, the ellipse excentricity is $e = (a^2 - b^2)^{0.5}/a$ (e near one means that the ellipse is flat, while $e = 0$ for a circle).

The inclination and the minor axis size are shown for R_{11} in figure 9. It can be seen that the inclination of the ellipses depends on the correlation level, and decreases (in absolute terms) when the level increases. Mean inclinations span between -15° and -6.5° from the levels 0.3 to 0.8, respectively. The structures are bent toward the high-speed flow, as it has already been noted by Mahadevan & Loth (1994) or Fleury *et al.* (2008). The minor axis size obviously increases when the correlation level of the contour increases. When non-dimensioned by the mixing layer momentum thickness, a constant value is found, which is in agreement with the linear growth of the turbulent length scales obtained above. The same features are also true for the major axis (not shown here). The axis lengths deliver another estimation for the size of the turbulent structures. For the contour of level 0.5, the ratios a/δ_θ and b/δ_θ are found to be 3 and 1.4, respectively. Translating this into a fraction of the mixing layer thickness δ ($\delta \approx 7.5\,\delta_\theta$) leads to 0.4 and 0.19. Thus, the turbulent structures can be described as *large*, in the acceptance of Papamoschou & Roshko (1988), since their size is of the same order of magnitude as the mixing layer thickness, but they do not extend over its entire width. The excentricity, not shown here, decreases when the correlation level increases, meaning that the contours of higher correlation level are closer to a circle than those of lower level. The excentricity values span from 0.91 to 0.83 for contour levels 0.3 to 0.8.

The results for R_{22} are not shown here for brevity. As compared to the case of R_{11}, the excentricity is smaller and the inclination is close to 90° (see Fleury *et al.* (2008)). Also, the axes of the ellipses are smaller, which is in agreement with the relation found between the different turbulent length scales.

CONCLUDING REMARKS

Particle image velocimetry has been applied to a choked jet of fully expanded Mach number $M_j = 1.10$. The strength of the shock-cell structure has been estimated on mean streamlines. The velocity gradients inside the jet plume wear off toward the mixing layer and in the downstream direction. Furthermore, velocity gradients typical of the shock-cell structure have still been observed in the subsonic part of the mixing layer.

The main part of this paper focused on the properties of turbulence. Overall, it has been found that the slightly underexpanded jet studied here behaves very similarly to jets at high subsonic Mach numbers. A simple method has been presented to compute the mixing layer momentum thickness δ_θ. Its evolution is fairly linear with the downstream distance, like for subsonic jets. No effect of the shock-cell pattern on δ_θ has been observed. The turbulence levels have been found to be approximately constant with downstream distance and very similar to those observed in subsonic jets. The location of the sonic line comparatively to the mixing layer centre and boundaries shows that the layer centre is located in its subsonic part. At the value of M_j investigated, only a small portion of the layer is at supersonic con-

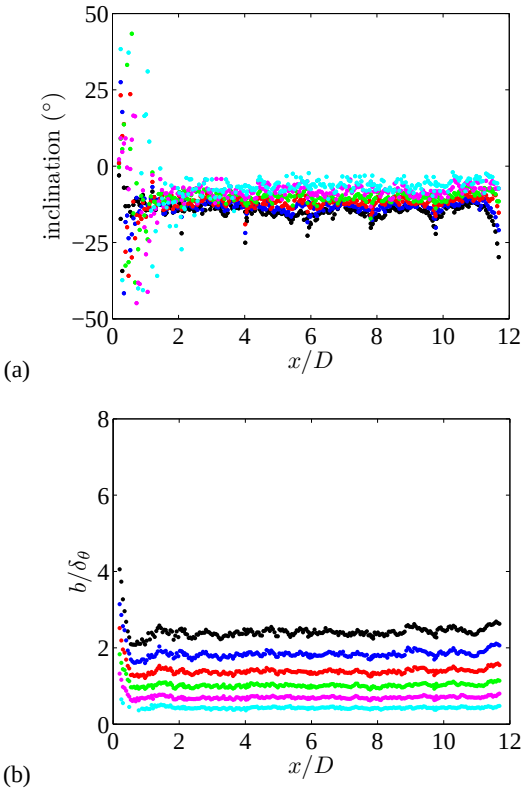

Figure 9. Evolution of the properties of the ellipses fitted to the correlation contours R_{11} ($M_j = 1.10$). (a) Inclination, (b) minor axis over δ_θ. Contour levels : • 0.3, • 0.4, • 0.5, • 0.6, • 0.7, • 0.8.

dition. It seems then that in this case, a non-negligible part of shock-associated noise could be produced in the subsonic region of the mixing layer. Spatial correlations of velocity fluctuations have been computed. A linear growth of the integral length scales has been obtained. The ratios of the growth rates of these scales to δ_θ take on similar values as in subsonic jets. The correlation contours have also been analysed as ellipses. The size of the structures thus defined is of the same order of magnitude as the local mixing layer thickness.

The data presented here could be used to investigate more precisely into the source term of the broadband shock-associated noise. To that end, a starting point could be the BBSAN model of Morris & Miller (2010). Evaluating the different parts of the source term inside the jet could shed light on the BBSAN source location, which is still not known precisely.

ACKNOWLEDGEMENTS

The authors wish to thank Airbus Operations SAS (Mauro Porta) and Snecma (Guillaume Bodard) for their joint financial support, as well as Jean-Michel Perrin and Nathalie Grosjean for their help in setting up the experiment and the PIV measurement system.

REFERENCES

Alkislar, M. B., Krothapalli, A. & Lourenco, L. M. 2003 Structure of a screeching rectangular jet : a stereoscopic particle image velocimetry study. *Journal of Fluid Mechanics* **489**, 121–154.

André, B., Castelain, T. & Bailly, C. 2011 Experimental study of flight effects on screech in underexpanded jets. *Physics of Fluids* **23**, 1–14.

André, B., Castelain, T. & Bailly, C. 2013*a* Broadband shock-associated noise in screeching and non-screeching underexpanded supersonic jets. *AIAA Journal* **51** (3), 665–673.

André, B., Castelain, T. & Bailly, C. 2013*b* Experimental exploration of underexpanded supersonic jets. *Accepted for publication in Shock Waves* .

Bridges, J. E. & Wernet, M. P. 2008 Turbulence associated with broadband shock noise in hot jets. NASA Technical Memorandum 215274.

Davies, P. O. A. L., Fisher, M. J. & Barratt, M. J. 1963 The characteristics of the turbulence in the mixing region of a round jet. *Journal of Fluid Mechanics* **15**, 337–367.

Fleury, V. 2006 Superdirectivité, bruit d'appariement et autres contributions au bruit de jet subsonique. PhD Thesis, Ecole Centrale de Lyon.

Fleury, V., Bailly, C., Jondeau, E., Michard, M. & Juvé, D. 2008 Space-time correlations in two subsonic jets using dual particle image velocimetry measurements. *AIAA Journal* **46** (10), 2498–2509.

Harper-Bourne, M. & Fisher, M. J. 1973 The noise from shock waves in supersonic jets. AGARD CP 131.

Jordan, P., Gervais, Y., Valière, J.-C. & Foulon, H. 2002 Jet exhaust aerodynamics and noise. E.U. Research Project Jean Deliverable 3.4.

Kerhervé, F., Jordan, P., Gervais, Y., Valière, J.-C. & Braud, P. 2004 Two-point laser doppler velocimetry measurements in a mach 1.2 cold supersonic jet for statistical aeroacoustic source model. *Experiments in Fluids* **37** (3), 419–437.

Laurence, J. C. 1956 Intensity, scale, and spectra of turbulence in mixing region of free subsonic jet. NACA Report 1292.

Mahadevan, R. & Loth, E. 1994 High-speed cinematography of compressible mixing layers. *Experiments in Fluids* **17** (3), 179–189.

Michalke, A. 1965 On spatially growing disturbances in an inviscid shear layer. *Journal of Fluid Mechanics* **23** (3).

Morris, P. J. & Miller, S. A. E. 2010 Prediction of broadband shock-associated noise using reynolds-averaged navier-stokes computational fluid dynamics. *AIAA Journal* **48** (12), 2931–2943.

Norum, T. D. & Seiner, J. M. 1982 Measurements of mean static pressure and far field acoustics of shock containing supersonic jets. NASA Technical Memorandum 84521.

Panda, J. & Seasholtz, R. G. 1999 Measurement of shock structure and shock-vortex interaction in underexpanded jets using rayleigh scattering. *Physics of Fluids* **11** (12), 3761–3777.

Papamoschou, D. & Roshko, A. 1988 The compressible turbulent shear layer: an experimental study. *Journal of Fluid Mechanics* **197**, 453–477.

Seiner, J. M. & Norum, T. D. 1980 Aerodynamic aspects of shock containing jet plumes. AIAA Paper 80-0965.

Seiner, J. M. & Yu, J. C. 1984 Acoustic near-field properties associated with broadband shock noise. *AIAA Journal* **22** (9), 1207–1215.

Troutt, T. R. & McLaughlin, D. K. 1982 Experiments on the flow and acoustic properties of a moderate-reynolds-number supersonic jet. *Journal of Fluid Mechanics* **116**.